LAWRENCE
LIVERMORE
NATIONAL
LABORATORY

UCRL-JRNL-222736

Gamma-ray production cross sections in multiple channels for neutron induced reaction on 48Ti for En=1 to 200 MeV

D. Dashdorj, G. E. Mitchell, P. E. Garrett, U. Agvaanluvsan, J. A. Becker, L. A. Bernstein, M. B. Chadwick, M. Devlin, N. Fotiades, T. Kawano, R. O. Nelson, W. Younes

July 11, 2006

Nuclear Science and Engineering

γ-ray production cross sections in multiple channels for neutron induced reaction on ^{48}Ti for E_n = 1 to 200 MeV

D. Dashdorj[†]

North Carolina State University, Raleigh, NC 27695
Lawrence Livermore National Laboratory, Livermore, CA 94551

G. E. Mitchell

North Carolina State University, Raleigh, NC 27695
Triangle Universities Nuclear Laboratory, Durham, NC 27708

J. A. Becker, U. Agvaanluvsan, L. A. Bernstein, and W. Younes

Lawrence Livermore National Laboratory, Livermore, CA 94551

P. E. Garrett

University of Guelph, Ont., Canada N1G 2W1

M. B. Chadwick, M. Devlin, N. Fotiades, T. Kawano, and R. O. Nelson

Los Alamos National Laboratory, Los Alamos, NM 87545

(Dated: November 9, 2006)

[†]Lawrence Livermore National Laboratory
L-414
7000 East Avenue
P.O.Box 808
Livermore, CA 94551
Fax number: 925-422-5940
Total 24 pages and 9 figures; Electronic address: dashdorj1@llnl.gov

Abstract

Prompt γ-ray production cross sections were measured on a ^{48}Ti sample for incident neutron energies from 1 MeV to 200 MeV. Partial γ-ray cross sections for transitions in $^{45-48}$Ti, $^{45-48}$Sc, and $^{43-45}$Ca were determined. The observation of about 130 transitions from 11 different isotopes in the present work provides a demanding test of reaction model calculations, and is the first study in this mass region to extract partial γ-ray cross sections for many different reaction channels over a wide range of incident neutron energies. The neutrons were produced by the Los Alamos National Laboratory spallation neutron source located at the LANSCE/WNR facility. The prompt-reaction γ rays were detected with the large-scale Compton-suppressed GErmanium Array for Neutron Induced Excitations (GEANIE). Event neutron energies were determined by the time-of-flight technique. The γ-ray excitation functions were converted to partial γ-ray cross sections and then compared with model calculations using the enhanced GNASH reaction code. Compound nuclear, preequilibrium emission and direct reaction mechanisms are included. Overall the model calculations of the partial γ-ray cross sections are in good agreement with measured values.

PACS numbers: 21.10.-i, 24.60.Dr, 25.40.-h, 25.40.Fq, 27.40.+z

I. INTRODUCTION

Neutron cross sections measured over a wide range of neutron energies from a few MeV up to several hundred MeV provide a unique data set to test sophisticated reaction modeling codes. This wide bombarding energy range can be obtained through the use of a pulsed spallation neutron source. The region above 10 MeV incident neutron energy where preequilibrium reactions are the dominant reaction mechanism has not been well explored with neutron-induced reactions. In the present work, a ^{48}Ti target was bombarded with neutrons up to 250 MeV and 11 different isotopic reaction products were observed. This data set provide a demanding test of reaction model calculations and it is the first study in this mass region to extract γ-ray excitation functions for many different reaction channels. The results of the present work are compared with enhanced GNASH reaction code calculations. GNASH code [1] employs Hauser-Feshbach calculations with both preequilibrium and direct reaction contributions. These calculations are sensitive to the accuracy of the level schemes, level density, γ-ray strength function, etc. Therefore model predictions with a Hauser-Feshbach code such as GNASH are challenging: for good agreement with experimental results, the theoretical descriptions must correctly predict the overall channel cross sections as well as correctly predicting angular momentum transfers and the resulting γ-ray cascades in the residual nuclei. Since the level scheme of ^{48}Ti is well known, without any low-lying isomeric states, comparison of experimental data with the GNASH calculations provides a good test of the nuclear reaction modeling employed.

In Section II the experimental procedure and data processing are described. The reaction model calculations are described in Section III. A discussion of the experimental results for reactions involving the 11 observed isotopes ($^{45-48}$Ti, $^{45-48}$Sc and $^{43-45}$Ca) is presented in Section IV. The final section provides a brief summary.

II. EXPERIMENTAL METHODS AND DATA ANALYSIS

The experimental data were obtained at the Los Alamos Neutron Science Center (LANSCE) Weapons Neutron Research (WNR) facility. At the WNR facility, spallation neutrons

are produced by bombarding a natural tungsten target with the 800-MeV pulsed proton beam from the LANSCE linac. The pulsed proton beam in this experiment consisted of micropulses 1.8-μs apart, bunched into macropulses 625-μs in duration. The widths of the micropulses and macropulses were less than 1 ns and 650 - 750 μs wide, respectively. Spallation neutrons with energies ranging from a few keV to nearly 800 MeV are produced. Beam-hardening material (1.5 cm of lead) was placed in the neutron flight path and charged particles were swept from the flight line by permanent magnets. The neutrons were collimated to a 1.5-cm diameter circular beam spot at the scattering-sample position. The scattering sample consisted of 3.3 grams of TiO_2 enriched to 99.81% ^{48}Ti in the form of a 2.4-cm diameter disk. The γ rays were detected with the GEANIE (GErmanium Array for Neutron Induced Excitations) spectrometer, located 20.34 m from the neutron source on the 60° right flight path. For this experiment, the GEANIE spectrometer consisted of 11 planar and 15 $\sim$ 20 - 25% High-purity Ge (HPGe) coaxial detectors. All of the planar detectors and 9 of the coaxial detectors were equipped with Compton suppression shields. The detectors were situated at a distance of $\sim$ 14 cm from the the scattering sample, which is located at the focal point of the spectrometer. The planar detectors were used to measure γ rays with energies less than 1 MeV and the coaxial detectors measured γ rays with energies up to 4 MeV. The planar detectors were arranged in rings at angles of 27.4° (four detectors), 58.4° (two detectors), 128.0° (one detector), and 142.7° (four detectors) with respect to the neutron beam direction. The coaxial detectors were arranged in rings at angles of 56.6° (two detectors), 77.7° (two detectors), 100.5° (four detectors), and 129.5° (one detector). The six remaining coaxial detectors were unsuppressed and their events were only analyzed in $\gamma\gamma$ coincidence mode. The data from the suppressed detectors were collected in singles-and-higher-fold mode, resulting in an average beam on array rate of $2 - 3$ kHz. The data stream consisted of a bit determining whether the event occurred in or out of the macropulse, the time relative to the start of the macropulse, the energy E_γ, and (if in beam) the time t_γ relative to the proton micropulse for each detector which recorded an event. A fission chamber with ^{235,238}U foils [2] was located 2 m upstream from the GEANIE spectrometer and fission chamber events were used to determine the neutron flux. Neutron energies were

determined by the time-of-flight (TOF) technique, using the detection time of the "flash" of γ rays caused by the spallation reaction with respect to the beam-rf signal as a reference marker. The detection time of γ rays produced by neutrons interacting with the sample was used to calculate the TOF of the neutrons relative to the micropulse time, measured by γ-flash detection. Similarly, signals from the fission chamber were used to provide a flight time relative to the γ-flash detection time (also observed in the fission chamber).

The data were collected for 6 days and a total of about 4.6×10^8 single- and higher-fold events were recorded. There were also separate experimental runs with $^{48}TiO_2$ "sandwiched" between 5-mil natural iron foils that were compared with the known ^{56}Fe(n,n$'\gamma$)^{56}Fe cross sections [3] in order to validate the experimental technique. During data playback, events were separated into beam-on and beam-off matrices. Two-dimensional matrices of E_γ vs. TOF and $\gamma\gamma$ coincidences were generated. Data from detectors of a particular type (planar or coaxial) were summed in order to improve statistics. The γ-ray detector energy calibration was performed using the energies of known transitions in ^{48}Ti and other isotopes in the beam-on data for each set of detectors. Figure 1 shows a γ-ray spectrum obtained with the coaxial Ge detectors, after selecting time gates corresponding to $E_n = 1 - 250$ MeV neutrons. This spectrum has more than 600 transitions from many different reaction channels plus background. There is a large background present from interactions of neutrons with the Ge crystals that obscure n + ^{48}Ti γ rays in some regions, e.g., near 600 keV.

The excitation functions were obtained by applying TOF gates 15 ns wide on the γ-ray events in the interval to $E_n = 1$ to 250 MeV. For each TOF bin, a 1D γ-ray pulse-height spectrum was generated and fitted with the computer code XGAM [4]; the peak shape parameters were determined from a global fit to the summed spectrum (Fig. 1). Fitted peaks in the spectrum were identified by comparison with accepted γ-ray energies, tabulated in the NUDAT database [5]. The identification of γ rays in GEANIE data can be complicated due to the large number of open reaction channels. The analysis of threshold energies in the γ-ray excitation functions was helpful in identifying and placing γ rays. Using the $\gamma\gamma$ coincidence matrix built during the data reduction a tentative level scheme for ^{48}Ti can be constructed. Multiplicity two-and-higher coincidences from both the planar and

coaxial detectors were sorted into a $4k \times 4k$ $\gamma\gamma$ matrix. Prompt coincidence events were considerably fewer compared to single-fold data; to maximize statistics the data from both planar and coaxial detectors were combined after converting them to the same energy range. To build the coincidence matrix, $\gamma\gamma$ resolving-time windows of 30 ns, 35 ns, and 40 ns were set for planar-planar, planar-coaxial and coaxial-coaxial detector coincidences, respectively. Coincidences between γ rays provide an additional tag to eliminate extraneous information in the spectra. The coincidence matrix was analyzed to confirm γ-ray assignments and to build a partial level scheme for ^{48}Ti.

Partial γ-ray cross sections for transitions were obtained using the following formula

$$\sigma_\gamma(E_n) = (1 + \alpha_\gamma) * \frac{\epsilon_{fc}}{\epsilon_{Ge}} * \frac{LT_{fc}}{LT_{Ge}} * \frac{1}{a_s} \frac{A_\gamma}{N_n}, \quad (1)$$

where α_γ is the internal conversion coefficient, ϵ_{Ge} and ϵ_{fc} are the detection efficiency of the Germanium detectors and fission chamber (respectively), LT_{Ge} and LT_{fc} are the live times of the Germanium detectors and fission chamber, a_s is the areal density of the ^{48}Ti sample, A_γ the γ - ray peak area, and N_n the number of neutrons counted in the fission chamber. The internal conversion coefficients are taken from the NUDAT [5] database. The neutron flux used in Eq. (1) can be determined from either the ^{235}U or the ^{238}U foil in the fission chamber. In this work, the ^{238}U foil in the fission chamber has been used consistently to extract partial γ-ray cross sections in order to minimize the "wrap-around" problem arising from the incident neutron beam structure (the flight path is long enough that low-energy neutrons arrive at the fission chamber location at the same time as high-energy neutrons from the next pulse). The pulse height and time-of-flight data from the ^{238}U fission chamber are shown in Fig. 2. In Fig. 2(a) the pulse-height spectrum is shown as determined from beam-on data. The vertical line indicates the lower limit of the gate taken on the pulse height in order to separate "α" events from fission events. In this case, "α" events include both those resulting from the natural α decay of ^{238}U and those originating from neutron-induced reactions on the backing material. Figure 2(b) shows the TOF spectrum obtained without any neutron gating conditions placed on the pulse-height spectrum. The TOF spectrum in Fig. 2(c) is fission gated, and it can be converted to a neutron intensity spectrum by using

the known ^{238}U(n,f) cross sections, and the efficiency for the fission detector is $\epsilon = 0.97$ [6]. The TOF bins correspond to the same neutron energies as for the γ-ray events, with the photofission events used as the reference time. The fission-chamber livetime is determined by taking the ratio of beam-on ADC events to the total number as given by a scalar-module count, gated by the beam macropulse envelope.

The γ-ray absolute efficiency curves for planar and coaxial detectors were calculated for GEANIE data using a Monte-Carlo simulation of the array [6]. The calculated efficiency curves are corrected for beam-profile and target-geometry effects. The Monte-Carlo simulations for coaxial detectors were performed for γ-ray energies between 300 keV and 1800 keV. The efficiency curve for the coaxial detectors was extrapolated to higher energies and verified with γ-ray reference sources. The deadtime fractions were calculated from the ratio of measured ADC and scaler counts. Total deadtimes of 62.0% and 58.0% were determined for the planar and coaxial sums, respectively, and deadtimes of 52.0% and 50.9% were obtained for the ^{235}U and ^{238}U fission foils.

As a validation of the experimental and analysis techniques, the partial cross sections of the $2_1^+ \rightarrow 0_1^+$ transition in ^{56}Fe was extracted from a series of runs with the ^{48}Ti sample sandwiched between 5-mil ^{nat}Fe foils. These data are compared to the evaluated cross section of 705 $\pm$ 56 mb at $E_n = 14.5$ MeV, determined by Nelson *et al.* [3]. The partial cross sections extracted for $2_1^+ \rightarrow 0_1^+$ transition from planar (σ_γ(847-keV) = 761 $\pm$ 42 mb) and coax (σ_γ(847-keV) = 742 $\pm$ 46 mb) data were consistent, within errors, with previous work.

III. THEORETICAL CALCULATIONS

Cross sections for ^{48}Ti + n reactions were calculated using the statistical Hauser-Feshbach reaction code GNASH [1]. The general calculational method assumes that the reaction proceeds in a series of sequential two-body breakup processes. At each stage in the reaction, γ-ray and particle emission are computed using Hauser-Feshbach theory, which conserves angular momentum and parity. Width fluctuation and preequilibrium corrections including

surface effects can be applied to the decay channels of the compound nucleus. The models utilized are expected to be most applicable for the energy range 1 keV to 150 MeV. Calculations were performed for ^{48}Ti + n reactions for neutron energies between 1 MeV and 120 MeV. Spherical optical model transmission coefficients for GNASH calculations were calculated with the CoH code by Kawano [7]. The CoH code solves the Schrödinger equation for a given optical potential, and calculates the differential elastic scattering, reaction and total cross sections, and transmission coefficients for neutron, proton, deuteron, triton, alpha particles. Optical model parameters are taken from global phenomenological models. For neutrons and protons the Koning and Delaroche [8] parameters were used. The potential of Becchetti and Greenlees [9] was used for deuterons and tritons and that of Avrigeanu [10] for α particles. The level density formulation of Ignatyuk [11] was utilized; this approach is particularly appropriate for analysis at higher excitation energies, since it includes the damping of shell effects in the level density parameter for increasing excitation energies. For γ-ray emission, the strength functions and photon transmission coefficients are obtained from the giant-resonance model of Kopecky and Uhl [12]. The standard giant-dipole-resonance (GDR) parameters are calculated for ^{48}Ti; σ_0 = 89.6 mb, E = 19.32 MeV and Γ = 5.80 MeV. For $M1$ radiation, the GDR parameters determined from systematics [12] are $E_0 = 41A^{-1/3}$ and Γ = 4 MeV. The excitation energy dependence of the γ-ray emission is included through the use of generalized Lorentzian forms for the $E1$, $M1$, and $E2$ strength functions. Width fluctuation corrections (WFC) using the Moldauer model [13] are included in GNASH calculations. After calculation of the population of the first compound nucleus using the Hauser-Feshbach expressions, corrections for preequilibrium and direct reaction effects are made. The exciton model includes an averaged squared matrix element for two-body interactions. Parameterization of the matrix element by Kalbach [14] includes one adjustable parameter, k, which was taken to be 170 MeV^3; this value was determined by adjusting the neutron emission spectrum at 14.1 MeV to the experimental data [15]. Multiple preequilibrium emission was included using the model of Ref. [16], and this does not have any adjustable parameters. Finally, direct reactions for neutron inelastic scattering were included for scattering to the 2_1^+ state in ^{48}Ti using the distorted-wave Born

approximation theory. The deformation parameters were taken from the compilation given in the International Atomic Energy Agency Reference Input Parameter Library (RIPL). The Koning-Delaroche optical potential [8] was used for the DWBA calculation.

IV. DISCUSSION

Excitation functions were extracted for a total of 11 different isotopes ($^{45-48}$Ti, $^{45-48}$Sc, and $^{43-45}$Ca); the lightest isotope was ^{43}Ca, which is populated via the $(n, \alpha 3n)$ reaction.

1 The Ti isotopes

Excitation functions were obtained for four Ti isotopes: ^{48}Ti, ^{47}Ti, ^{46}Ti and ^{45}Ti. The experimental partial cross sections for individual γ-rays are compared with the GNASH calculations for these nuclei in Figs. 3-5. The overall agreement was excellent, especially for the $(n, n'\gamma)$ channel at neutron energies up to 20 MeV. The measured $(n, n'\gamma)$ cross section for the 983-keV 2^+ to $0^+ g.s.$ transition in ^{48}Ti (which accounts for most of the total inelastic cross section) is higher than calculated for neutron energies above 25 MeV (see Fig. 3). Much of this discrepancy may be due to preequilibrium effects in the experimental data. A similar calculated underprediction occurred in several previous cases – ^{207,208}Pb$(n, xn\gamma)$ [17], ^{92}Mo$(n, xnypz\alpha\gamma)$ [18], and ^{196}Pt$(n, xnyp\gamma)$ [19] – the last two investigated using the GEANIE array. Most of the transitions in the $(n, n'\gamma)$ reaction channel are in excellent agreement with theoretical calculations.

Partial γ-ray cross sections as a function of E_n in the $(n, 2n\gamma)$ reaction channel are shown in Fig. 4. For the transition between the first-excited state and the ground state in ^{47}Ti the calculations overpredict the experimental data above the threshold energy. In this incident neutron energy region, the preequilibrium reaction plays an important role. Unlike this overprediction for ground and first-excited state, the GNASH calculation underpredicts the $11/2^-$ to $7/2^-$ and $3/2^+$ to $5/2^- g.s.$ transitions. The reason for this discrepancy is unknown. The excitation functions for the lighter Ti isotopes, shown in Fig. 5, are in reasonable overall agreement with the GNASH calculations in both shape and magnitude. For ^{45}Ti, the cross

sections do not fall as rapidly as the calculations suggest. However, it is satisfying that the portion of the excitation function dominated by compound processes is well reproduced.

2 The Sc isotopes

Partial γ-ray cross sections were obtained for four Sc isotopes: ^{48}Sc, ^{47}Sc, ^{46}Sc and ^{45}Sc. These isotopes were strongly populated by reactions ranging from the (n,p) channel to the $(n,4np)$ channel. Cross sections for transitions in these Sc nuclei are shown in Figs. 6–8. As is evident from Fig. 6, the excitation functions for the (n,p) channel are in good agreement with the GNASH predictions. The excitation functions show the typical behavior characteristic of a charged-particle-exit channel, i.e., near the threshold, the excitation functions rise slower than those of the neutron exit channel. This is due to the Coulomb barrier inhibiting the evaporation of charged particles. The (n,p) Q value is -3.21 MeV, although most of the ^{48}Sc γ rays are not observed until ≈ 5 MeV, indicating that approximately 2 MeV excitation energy is required before protons are evaporated.

^{47}Sc is the heaviest Sc isotope where composite particles can be emitted from the compound system ^{49}Ti. The difference in the thresholds between the (n,d) and (n,np) reactions is 2.27 MeV. Shown in Fig. 7 are results for transitions in the ^{47}Sc nuclei. Since none of the prompt γ rays are observed below the (n,np) threshold of 11.7 MeV, there is no evidence for deuteron emission at low neutron bombarding energies, nor it is expected. The observed transition between $3/2^-_1$ to $7/2^- g.s.$ levels in ^{47}Sc was about a factor of two higher than the model prediction. In the experiment, this line is located close to the "neutron bump" (neutrons interact with germanium crystals so the spectra is broadened) therefore it might have been contaminated by it.

Excitation functions for transitions from the lightest Sc nuclei observed in the present work, ^{46}Sc and ^{45}Sc, are shown in Fig. 8. Of interest is the threshold behavior of the excitation functions: they increase more slowly than the calculations predict.

Excitation functions were obtained for γ rays from ^{45}Ca, ^{44}Ca and ^{43}Ca. The reactions are complicated: α emission competes with the emission of two protons and two neutrons. Experimental cross sections and GNASH calculations for the Ca isotopes are shown in Fig. 9. In general the calculations are in good agreement with the experimental excitation functions, especially the general shape. The calculated partial cross sections show a definite double-humped structure, which is attributed to α emission at low incident neutron energies followed by contributions from $2p2n$ emission for higher neutron energies. The physical threshold for an α emission channel is higher than the kinematic threshold due to the Coulomb barrier. Shown in Fig. 9 are excitation functions for transitions assigned to ^{45}Ca, ^{44}Ca and ^{43}Ca. In the first panel, the calculation underpredicts the 174-keV $5/2^-$ to $7/2^-$ ground-state transition. For the 4^+ to 2^+ and 2^+ to 0^+ transitions in the $(n, n\alpha/3n2p)$ channel, the adjustment of the level density parameters may improve the predictions of the $(n, n\alpha)$ channel, but at the expense of the good description of the $(n, 3n2p)$ channel. The shapes of the cross sections for transitions in high particle multiplicity reactions are reproduced reasonably well. It is interesting to note that both cross sections still have an observable dip between the $(n, xn\alpha)$ and $[n, (x+2)n2p]$ channels.

V. SUMMARY AND CONCLUSION

Excitation functions of prompt γ rays produced in the n+^{48}Ti reaction have been measured using the GEANIE spectrometer at the LANSCE/WNR facility. The individual γ-ray yields have been converted to partial γ-ray cross sections as a function of incident neutron energy; this conversion includes accounting for neutron flux, sample thickness, deadtime corrections, detector and fission chamber efficiencies, and internal conversion processes. The experimental data are presented for neutron energies up to 200 MeV and γ rays from a total of 11 different isotopes, $^{45-48}$Ti, $^{45-48}$Sc and $^{43-45}$Ca, were observed and the predominant partial γ-ray cross sections extracted. These partial γ-ray cross sections were compared with calculations performed with the GNASH reaction code. The GNASH calculations reproduce

the shape and magnitude of most transitions reasonably well, but there are significant deviations in the preequilibrium regime. It is speculated that most of the prediction shortcomings are due to modeling the γ-ray cascade, including angular-momentum transfer effects, and in treating preequilibrium reaction mechanisms. We plan to examine the impact of improved understanding of preequilibrium reaction models. Measuring the prompt reaction γ rays as a function of incident neutron energy may provide better understanding of the spin distribution populated by the preequilibrium reaction. This information can be obtained by studying angular momentum information for the γ-ray cascades in the residual nucleus.

VI. ACKNOWLEDGMENTS

This work was supported by in part by the U.S. Department of Energy Grants No. DE-FG52-06NA26194 and No. DE-FG02-97-ER41042, and was performed under the auspices of the U.S. Department of Energy by the University of California, Lawrence Livermore National Laboratory and Los Alamos National Laboratory under contract Nos. W-7405-ENG-48 and W-7405-ENG-36, respectively. This work has benefited from the use of the LANSCE accelerator facility, supported under DOE contract No. W-7405-ENG-36.

REFERENCES

[1] P. G. Young, E. D. Arthur, and M. B. Chadwick, Tech. Rep. LA-12343-MS, Los Alamos National Laboratory (1992).

[2] S. A. Wender, S. Balestrini, A. Brown, R. C. Haight, C. M. Laymon, T. M. Lee, P. W. Lisowski, W. McCorkle, R. O. Nelson, W. Parker, and N. Hill, Nucl. Instrum. Methods Phys. Res. A **336**, 226 (1993).

[3] R. O. Nelson, N. Fotiades, M. Devlin, J. A. Becker, P. E. Garrett, and W. Younes, in *International Conference on Nuclear Data for Science and Technology*, edited by R. C. Haight, M. B. Chadwick, T. Kawano, and P. Talou (American Institute of Physics, 2005), p. 838.

[4] W. Younes, *The XGAM peak-fitting program*, manuscript in preparation.

[5] National Nuclear Data Center, Information extracted from the NuDat database, http://www.nndc.bnl.gov/nudat2.

[6] D. P. McNabb, Tech. Rep. UCRL-ID-139906, Lawrence Livermore National Laboratory (1999).

[7] T. Kawano (2005), private communication.

[8] A. J. Koning and J. P. Delaroche, Nucl. Phys. A **713**, 231 (2003).

[9] F. D. Becchetti and G. W. Greenlees, in *Polarization Phenomena in Nuclear Reactions*, edited by H. H. Barschall and W. Haeberli (University of Wisconsin Press, Madison, 1971), p. 682.

[10] V. Avrigeanu, P. E. Hodgson, and M. Avrigeanu, Phys. Rev. **C 49**, 2136 (1994).

[11] A. V. Ignatyuk, G. N. Smirenkin, and A. S. Toshin, Sov. J. Nucl. Phys. **21**, 255 (1975).

[12] J. Kopecky and M. Uhl, Phys. Rev. **C 41**, 1941 (1989).

[13] P. A. Moldauer, Nucl. Phys. **A 344**, 185 (1980).

[14] C. Kalbach, Phys. Rev. **C32**, 1157 (1985).

[15] M. Baba, M. Ishikawa, N. Yabuta, T. Kikuchi, H. Wakabayashi, and N. Hirakawa, in *Proc. Int. Conf. Nuclear Data for Science and Techology*, edited by S. Igarasi (Mito, Japan, 1988), p. 291.

[16] M. B. Chadwick, P. G. Young, D. C. George, and Y. Watanabe, Phys. Rev. **C50**, 996 (1994).

[17] H. Vonach, A. Pavlik, M. B. Chadwick, R. C. Haight, R. O. Nelson, S. A. Wender, and P. G. Young, Phys. Rev. **C 50**, 1952 (1994).

[18] P. E. Garrett, L. A. Bernstein, J. A. Becker, K. Hauschild, C. A. McGrath, D. P. McNabb, W. Younes, M. B. Chadwick, G. D. Johns, R. O. Nelson, W. S. Wilburn, E. Tavukcu, *et al.*, Phys. Rev. **C 62**, 054608 (2000).

[19] E. Tavucku, L. A. Bernstein, K. Hauschild, J. A. Becker, P. E. Garrett, C. A. McGrath, D. P. McNabb, W. Younes, M. B. Chadwick, R. O. Nelson, G. D. Johns, and G. E. Mitchell, Phys. Rev. **C 64**, 054614 (2001).

FIG.1: Spectrum obtained from the sum of the coaxial detectors for the ^{48}Ti(n,xγ) reaction. The condition on the time of flight corresponds to E_n= 1 – 250 MeV neutrons. Some of the prominent transitions in the residual nuclei are labeled by their energy in keV and residual nucleus.

FIG.2: Spectrum from the ^{238}U fission foil used to determine the neutron intensity at the GEANIE spectrometer. In panel (a) the pulse height spectrum is shown. The vertical line corresponds to the lower limit on the pulse-height gate for a signal to be considered a fission event. In panel (b) the raw TOF spectrum is shown. The time of the events is measured relative to the proton beam burst. In panel (c) the TOF spectrum resulting from imposing the condition in panel (a) is shown.

FIG.3: Measured partial γ-ray cross sections for E_γ = 983-keV, 1312-keV, 1037-keV, and 1437-keV transitions in the ^{48}Ti$(n,n'\gamma)^{48}$Ti reaction for neutron energies between 1 and 200 MeV. The solid lines represent the GNASH calculations for the partial γ-ray transitions.

FIG.4: Measured partial γ-ray cross sections for E_γ = 159-keV, 1093-keV, 1285-keV, and 2260-keV transitions in the ^{48}Ti$(n,2n\gamma)^{47}$Ti reaction for neutron energies between 10 to 200 MeV. The solid lines represent the GNASH calculations for the partial γ-ray transitions.

FIG.5: Measured partial γ-ray cross sections for E_γ = 889-keV, 1120-keV transitions in the ^{48}Ti$(n,3n\gamma)^{46}$Ti reaction and E_γ = 293-keV, 414-keV transitions in the ^{48}Ti$(n,4n\gamma)^{45}$Ti reaction for neutron energies between 10 and 200 MeV. The solid lines represent the GNASH calculations for the partial γ-ray transitions.

FIG:6: Measured partial γ-ray cross sections for E_γ = 121-keV, 131-keV, 370-keV, and 520-keV transitions in the ^{48}Ti(n,pγ)^{48}Sc reaction for neutron energies between 1 and 200 MeV. The solid lines represent the GNASH calculations for the partial γ-ray transitions.

FIG.7: Measured partial γ-ray cross sections for E_γ = 808-keV, 1147-keV, 1297-keV, and 1404-keV transitions in the ^{48}Ti(n,pγ)^{47}Sc reaction for neutron energies between 1 and 200 MeV. The solid lines represent the GNASH calculations for the partial γ-ray transitions.

FIG.8: Measured partial γ-ray cross sections for E_γ = 229-keV and 295-keV transitions in the ^{48}Ti(n,2npγ)^{46}Sc reaction and for the E_γ = 543-keV and 1056-keV transitions in the ^{48}Ti(n,3npγ)^{45}Sc reaction for neutron energies between 10 to 200 MeV. The solid lines

represent the GNASH calculations for the partial γ-ray transitions.

FIG.9: Measured partial cross sections for the E_γ = 174-keV transition from the ^{48}Ti(n,$\alpha/2n2p\gamma$)^{45}Ca reaction, the E_γ = 1126-keV and 1157-keV transitions from the ^{48}Ti(n,n$\alpha/3n2p\gamma$)^{44}Ca reaction, and the E_γ = 373-keV transition in the ^{48}Ti(n,2n$\alpha/4n2p\gamma$)^{43}Ca reaction for neutron energies between 10 to 200 MeV. The solid lines represent the GNASH calculations for the partial γ-ray transitions.

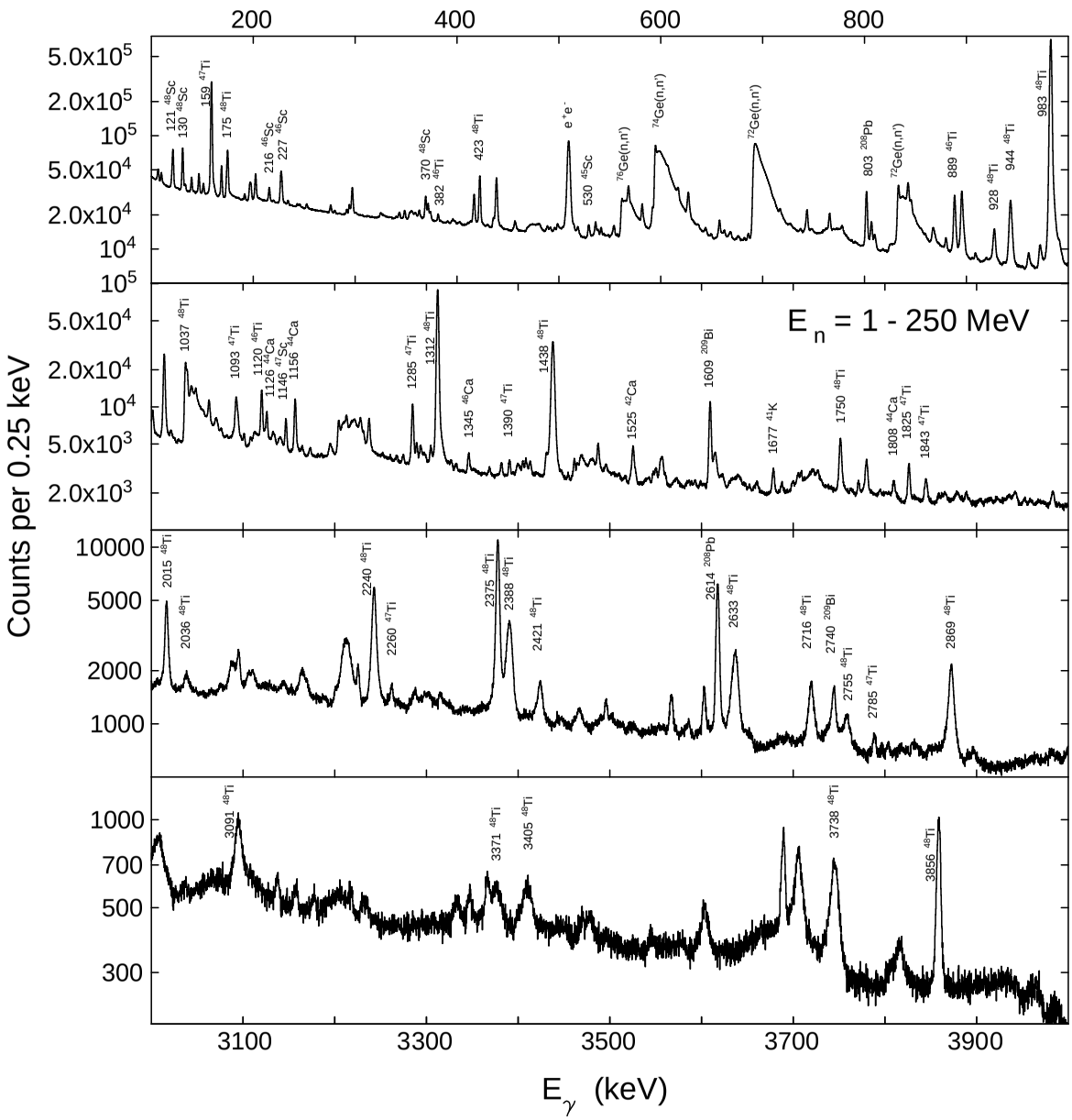
Counts per 0.25 keV
E_γ (keV)
E_n = 1 - 250 MeV
200
400
600
800
3100
3300
3500
3700
3900
5.0x10^5
2.0x10^5
10^5
5.0x10^4
2.0x10^4
10^4
5.0x10^3
2.0x10^3
10000
5000
2000
1000
700
500
300
121 45Sc
130 46Sc
159 47Ti
175 48Ti
216 46Sc
227 46Sc
370 48Sc
382 48Ti
423 48Ti
e+e-
530 45Sc
76Ge(n,n')
74Ge(n,n')
72Ge(n,n')
803 208Pb
889 46Ti
928 48Ti
944 48Ti
983 48Ti
1037 48Ti
1093 47Ti
1120 46Ti
1126 44Ca
1146 47Sc
1156 44Ca
1285 47Ti
1312 48Ti
1345 46Ca
1390 47Ti
1438 48Ti
1525 42Ca
1609 209Bi
1677 41K
1750 48Ti
1808 44Ca
1825 47Ti
1843 47Ti
2015 48Ti
2036 48Ti
2240 48Ti
2260 47Ti
2375 48Ti
2388 48Ti
2421 48Ti
2614 208Pb
2633 48Ti
2716 48Ti
2740 209Bi
2755 45Ti
2785 47Ti
2869 48Ti
3091 48Ti
3371 48Ti
3405 48Ti
3738 48Ti
3856 48Ti

FIG. 1:

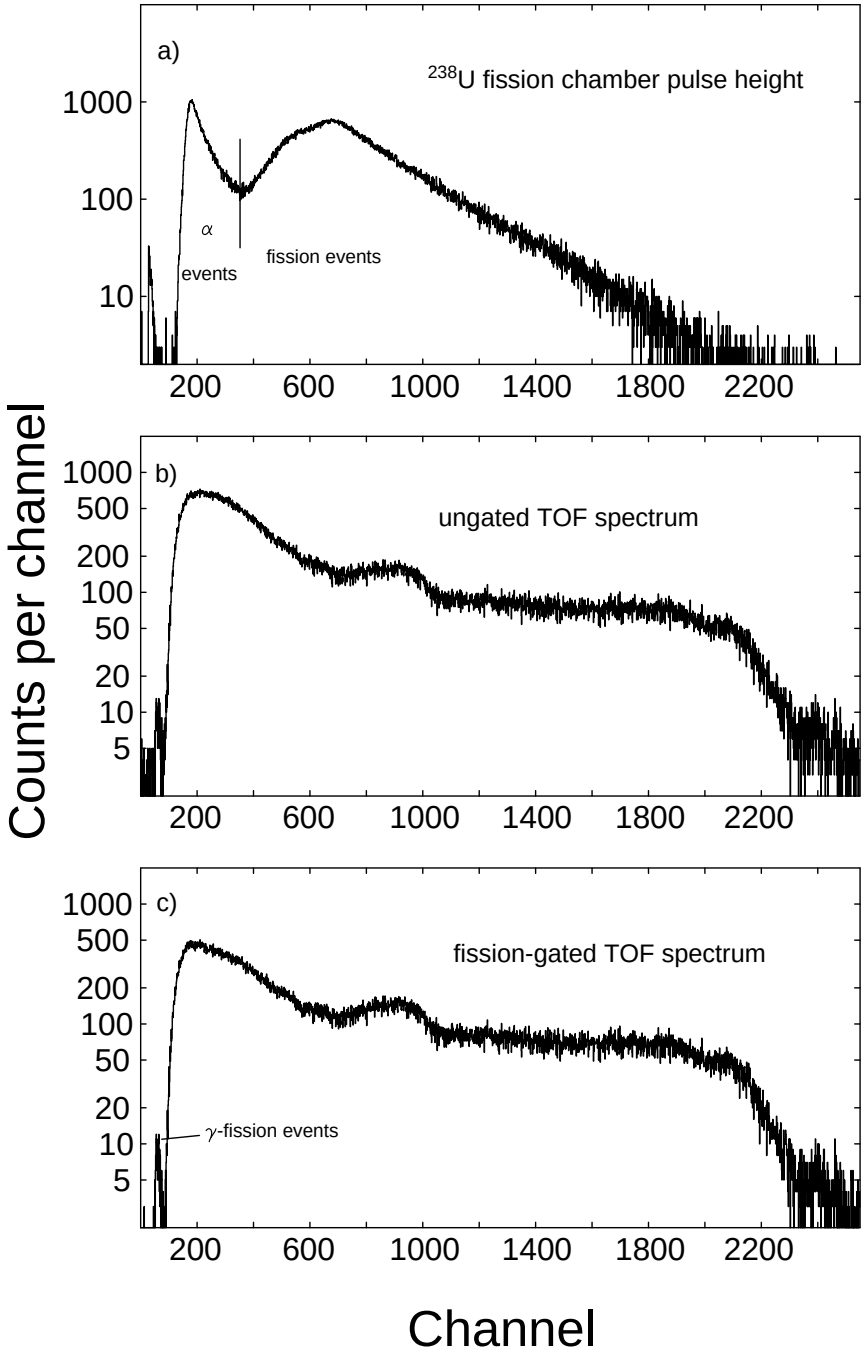
a)
^{238}U fission chamber pulse height
1000
100
10
α
events
fission events
200
600
1000
1400
1800
2200
b)
ungated TOF spectrum
1000
500
200
100
50
20
10
5
c)
fission-gated TOF spectrum
γ-fission events
Counts per channel
Channel

FIG. 2:

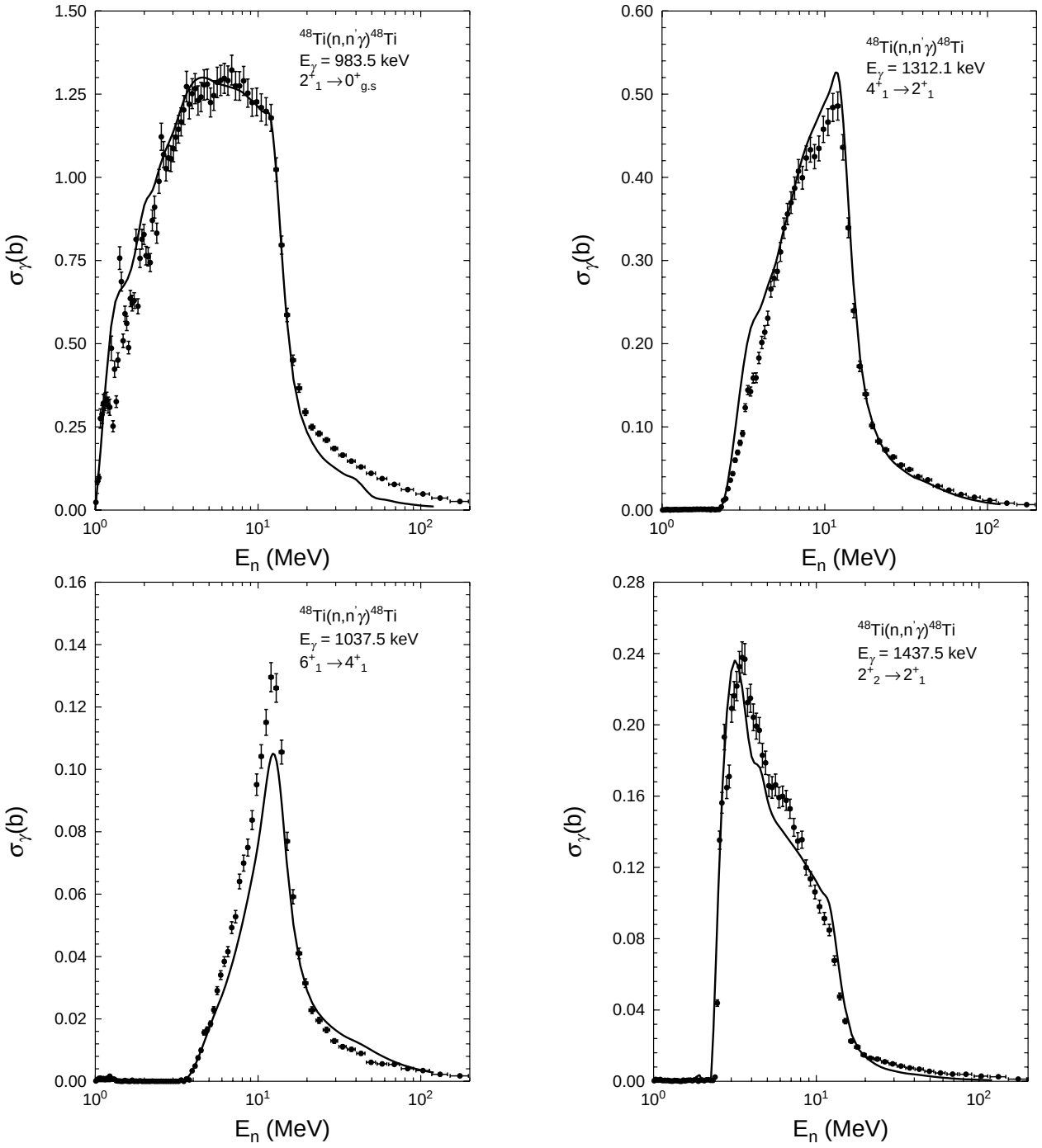
^{48}Ti(n,n'γ)^{48}Ti
E_γ = 983.5 keV
$2^+_1 \rightarrow 0^+_{g.s}$
^{48}Ti(n,n'γ)^{48}Ti
E_γ = 1312.1 keV
$4^+_1 \rightarrow 2^+_1$
^{48}Ti(n,n'γ)^{48}Ti
E_γ = 1037.5 keV
$6^+_1 \rightarrow 4^+_1$
^{48}Ti(n,n'γ)^{48}Ti
E_γ = 1437.5 keV
$2^+_2 \rightarrow 2^+_1$
σ_γ(b)
E_n (MeV)

FIG. 3:

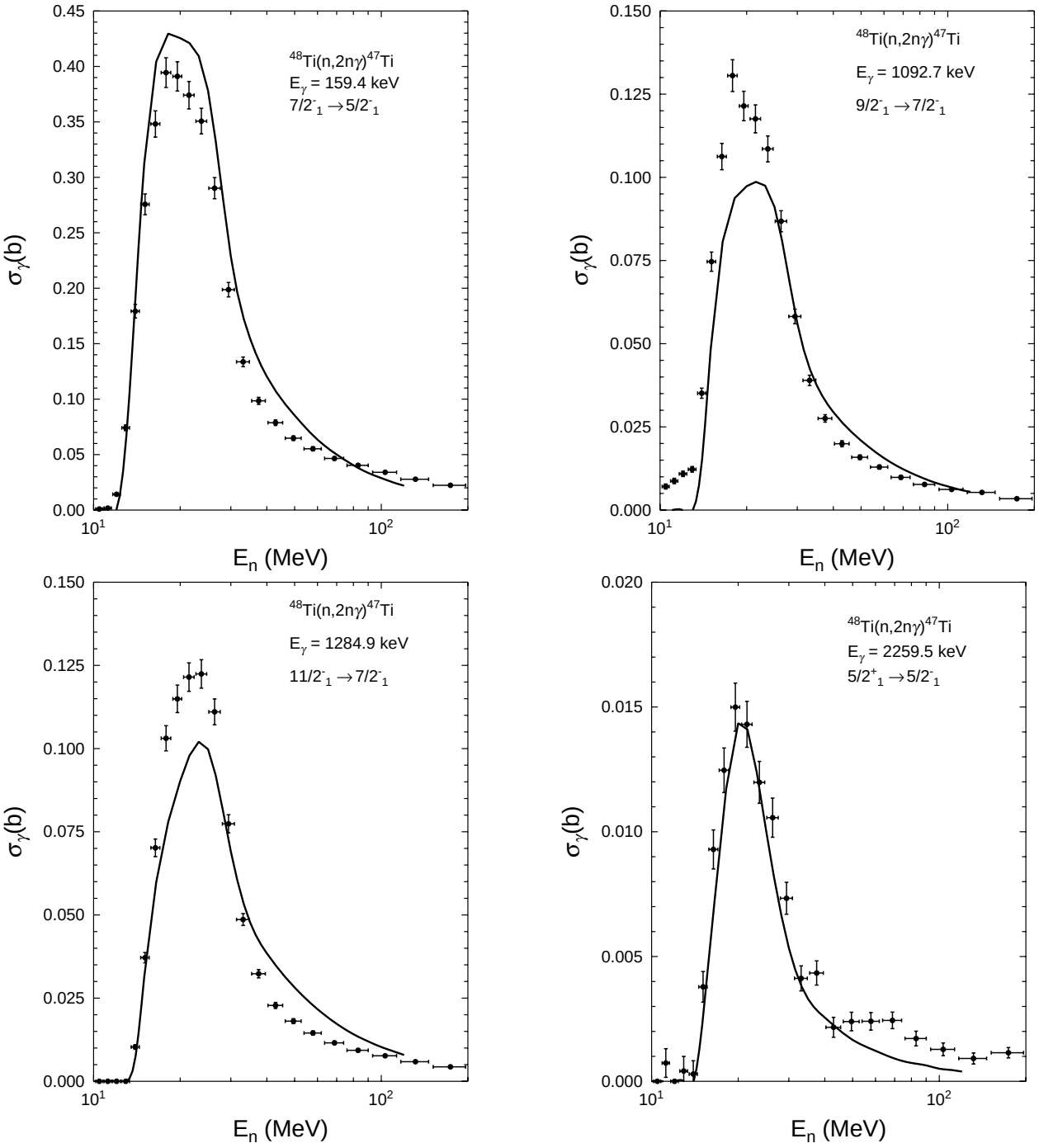
^{48}Ti(n,2nγ)^{47}Ti
E_γ = 159.4 keV
$7/2^-_1 \rightarrow 5/2^-_1$
^{48}Ti(n,2nγ)^{47}Ti
E_γ = 1092.7 keV
$9/2^-_1 \rightarrow 7/2^-_1$
^{48}Ti(n,2nγ)^{47}Ti
E_γ = 1284.9 keV
$11/2^-_1 \rightarrow 7/2^-_1$
^{48}Ti(n,2nγ)^{47}Ti
E_γ = 2259.5 keV
$5/2^+_1 \rightarrow 5/2^-_1$
σ_γ(b)
E_n (MeV)

FIG. 4:

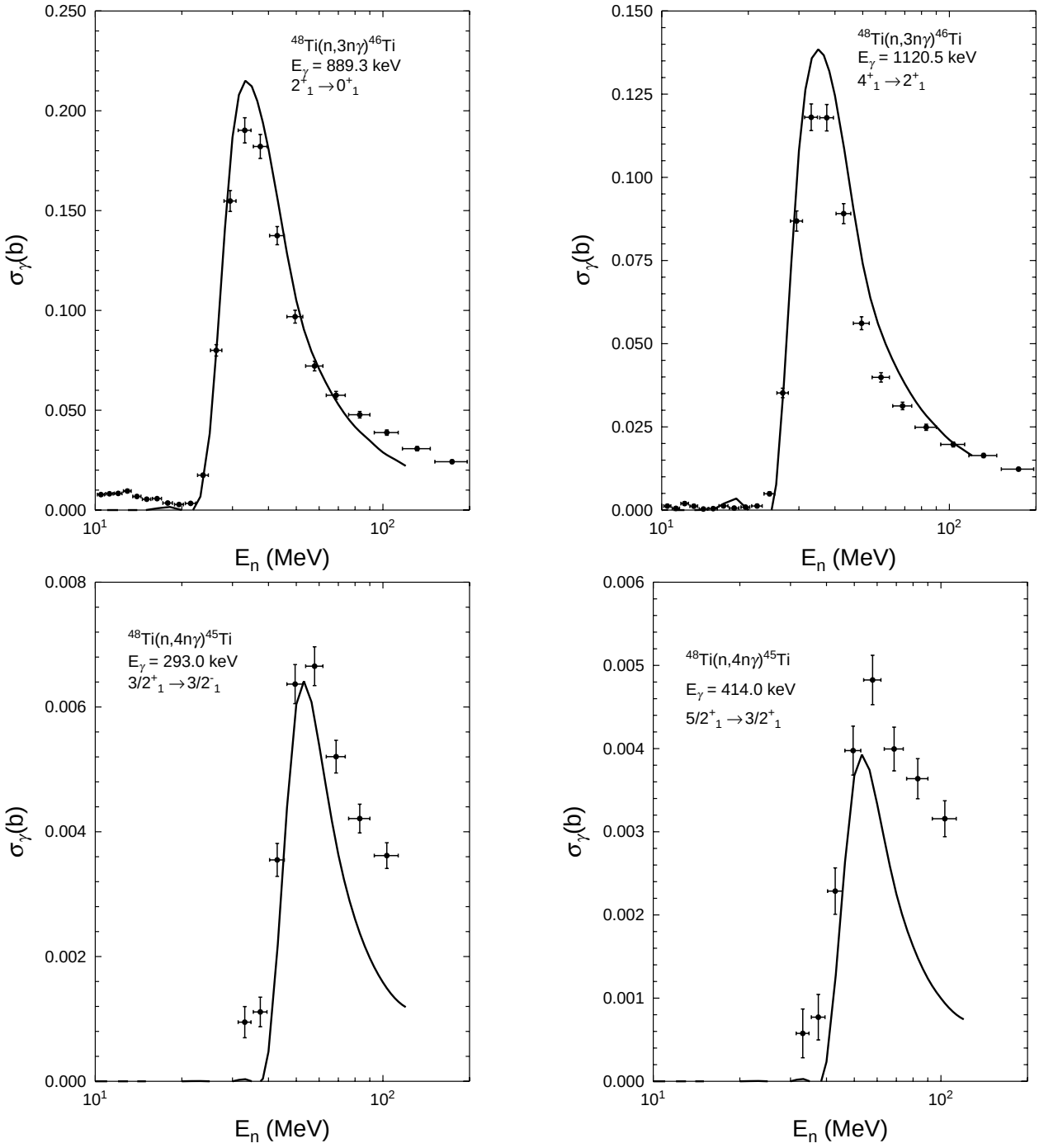
^{48}Ti(n,3nγ)^{46}Ti
E_γ = 889.3 keV
$2^+_1 \rightarrow 0^+_1$
^{48}Ti(n,3nγ)^{46}Ti
E_γ = 1120.5 keV
$4^+_1 \rightarrow 2^+_1$
^{48}Ti(n,4nγ)^{45}Ti
E_γ = 293.0 keV
$3/2^+_1 \rightarrow 3/2^-_1$
^{48}Ti(n,4nγ)^{45}Ti
E_γ = 414.0 keV
$5/2^+_1 \rightarrow 3/2^+_1$
σ_γ(b)
E_n (MeV)

FIG. 5:

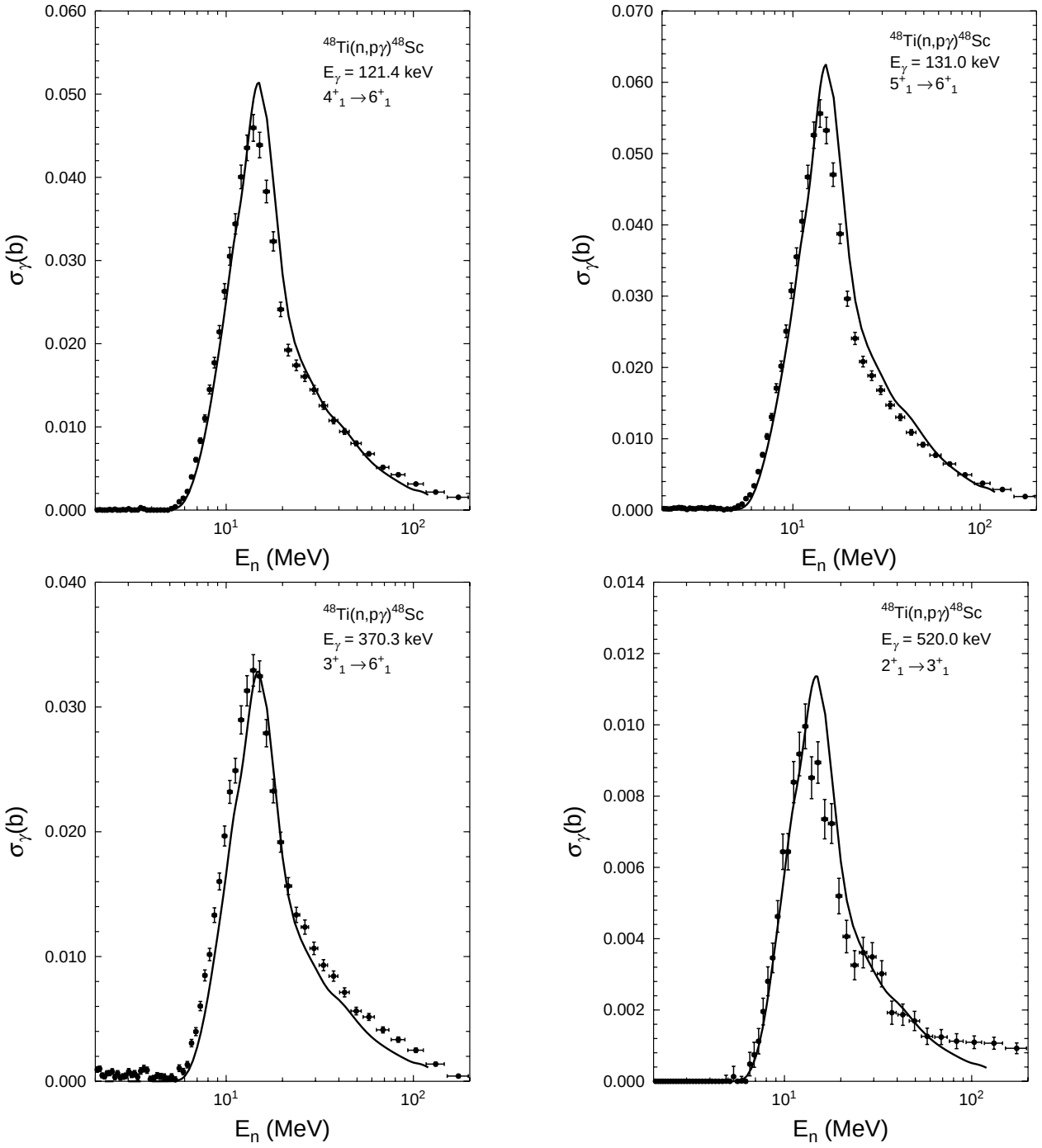
^{48}Ti(n,pγ)^{48}Sc
E_γ = 121.4 keV
$4^+_1 \rightarrow 6^+_1$
^{48}Ti(n,pγ)^{48}Sc
E_γ = 131.0 keV
$5^+_1 \rightarrow 6^+_1$
^{48}Ti(n,pγ)^{48}Sc
E_γ = 370.3 keV
$3^+_1 \rightarrow 6^+_1$
^{48}Ti(n,pγ)^{48}Sc
E_γ = 520.0 keV
$2^+_1 \rightarrow 3^+_1$
σ_γ(b)
E_n (MeV)

FIG. 6:

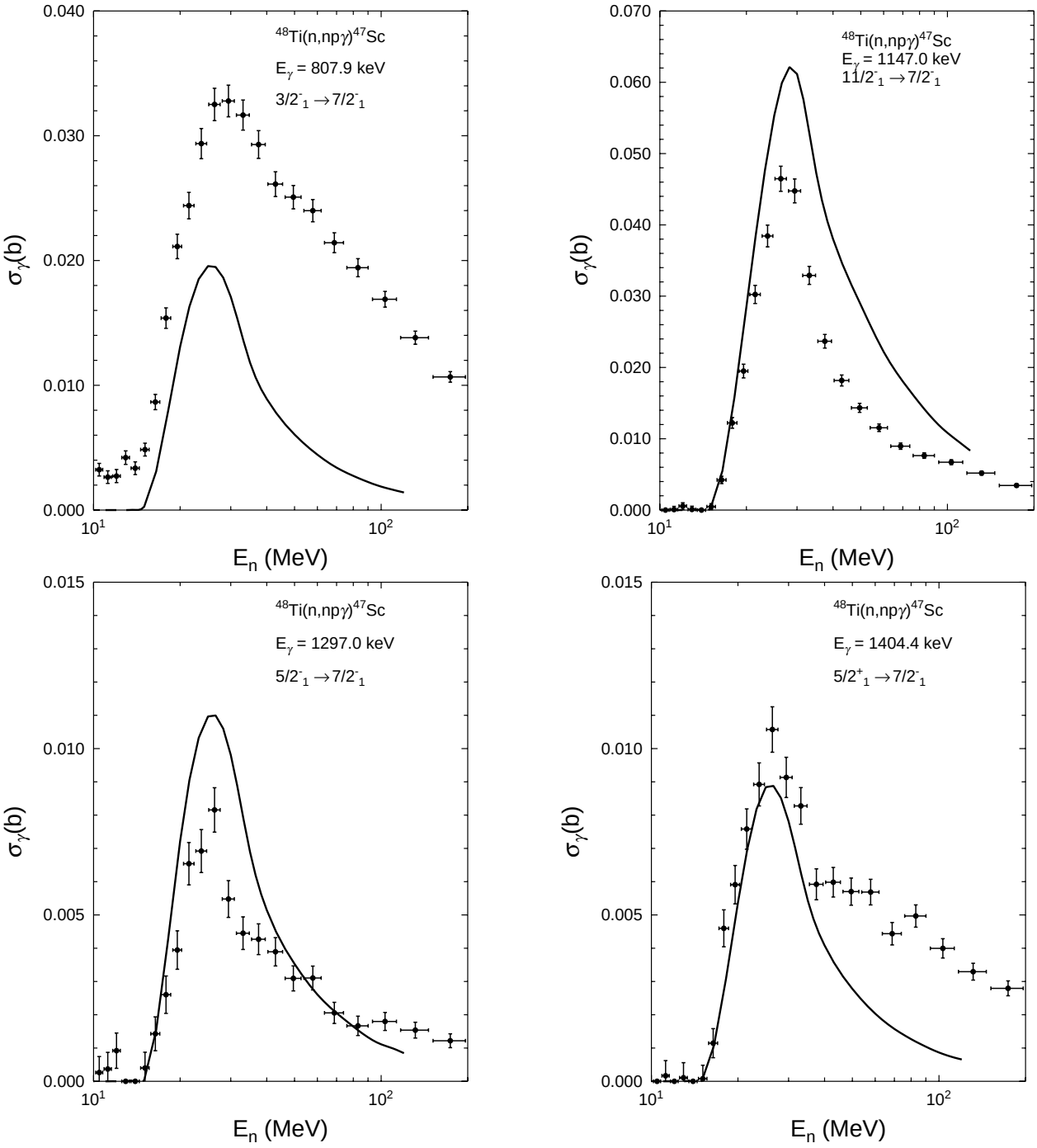
^{48}Ti(n,npγ)^{47}Sc
E_γ = 807.9 keV
$3/2^-_1 \rightarrow 7/2^-_1$
^{48}Ti(n,npγ)^{47}Sc
E_γ = 1147.0 keV
$11/2^-_1 \rightarrow 7/2^-_1$
^{48}Ti(n,npγ)^{47}Sc
E_γ = 1297.0 keV
$5/2^-_1 \rightarrow 7/2^-_1$
^{48}Ti(n,npγ)^{47}Sc
E_γ = 1404.4 keV
$5/2^+_1 \rightarrow 7/2^-_1$
σ_γ(b)
E_n (MeV)

FIG. 7:

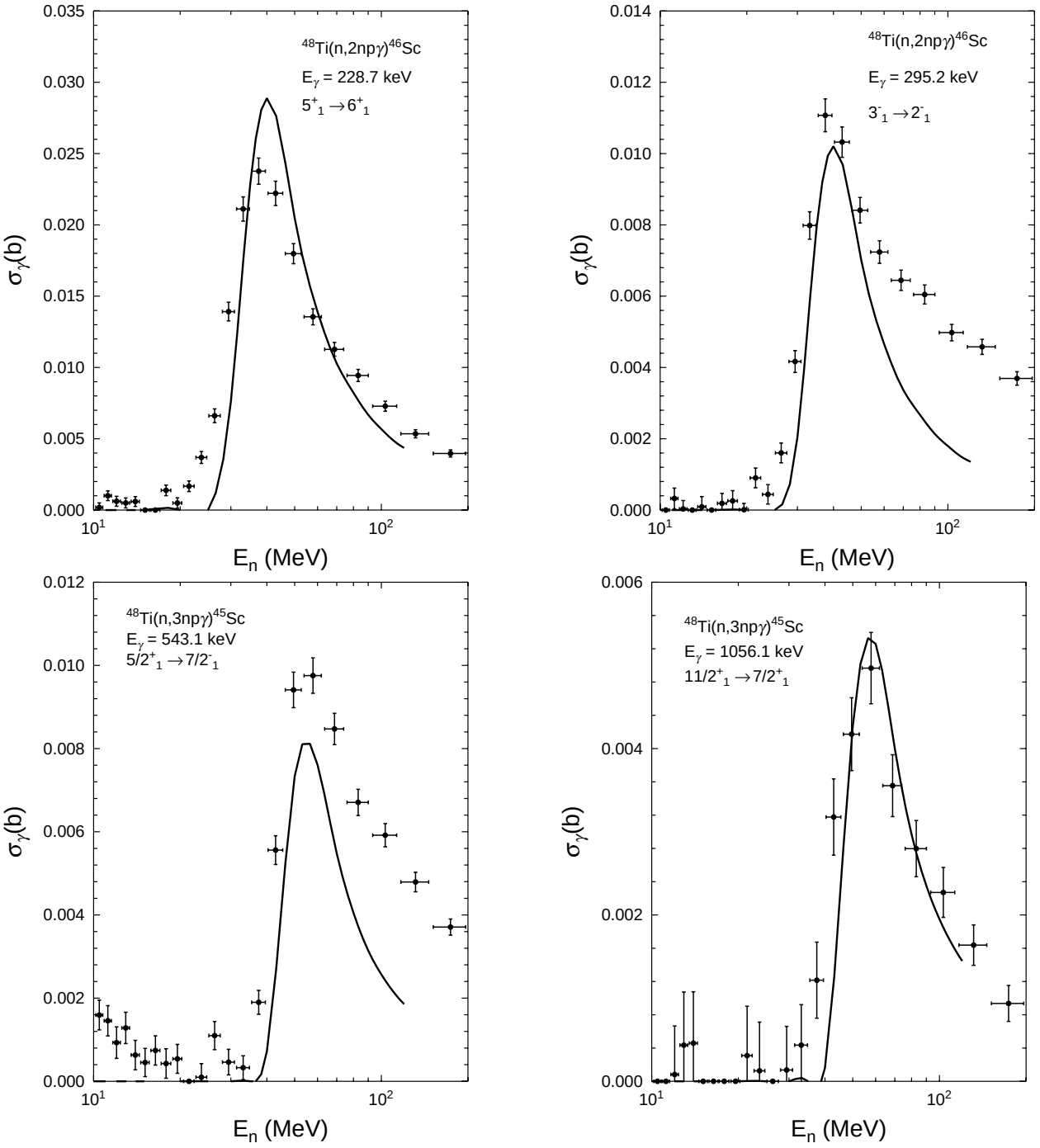
^{48}Ti(n,2npγ)^{46}Sc
E_γ = 228.7 keV
$5^+_1 \rightarrow 6^+_1$
^{48}Ti(n,2npγ)^{46}Sc
E_γ = 295.2 keV
$3^-_1 \rightarrow 2^-_1$
^{48}Ti(n,3npγ)^{45}Sc
E_γ = 543.1 keV
$5/2^+_1 \rightarrow 7/2^-_1$
^{48}Ti(n,3npγ)^{45}Sc
E_γ = 1056.1 keV
$11/2^+_1 \rightarrow 7/2^+_1$
σ_γ(b)
E_n (MeV)

FIG. 8:

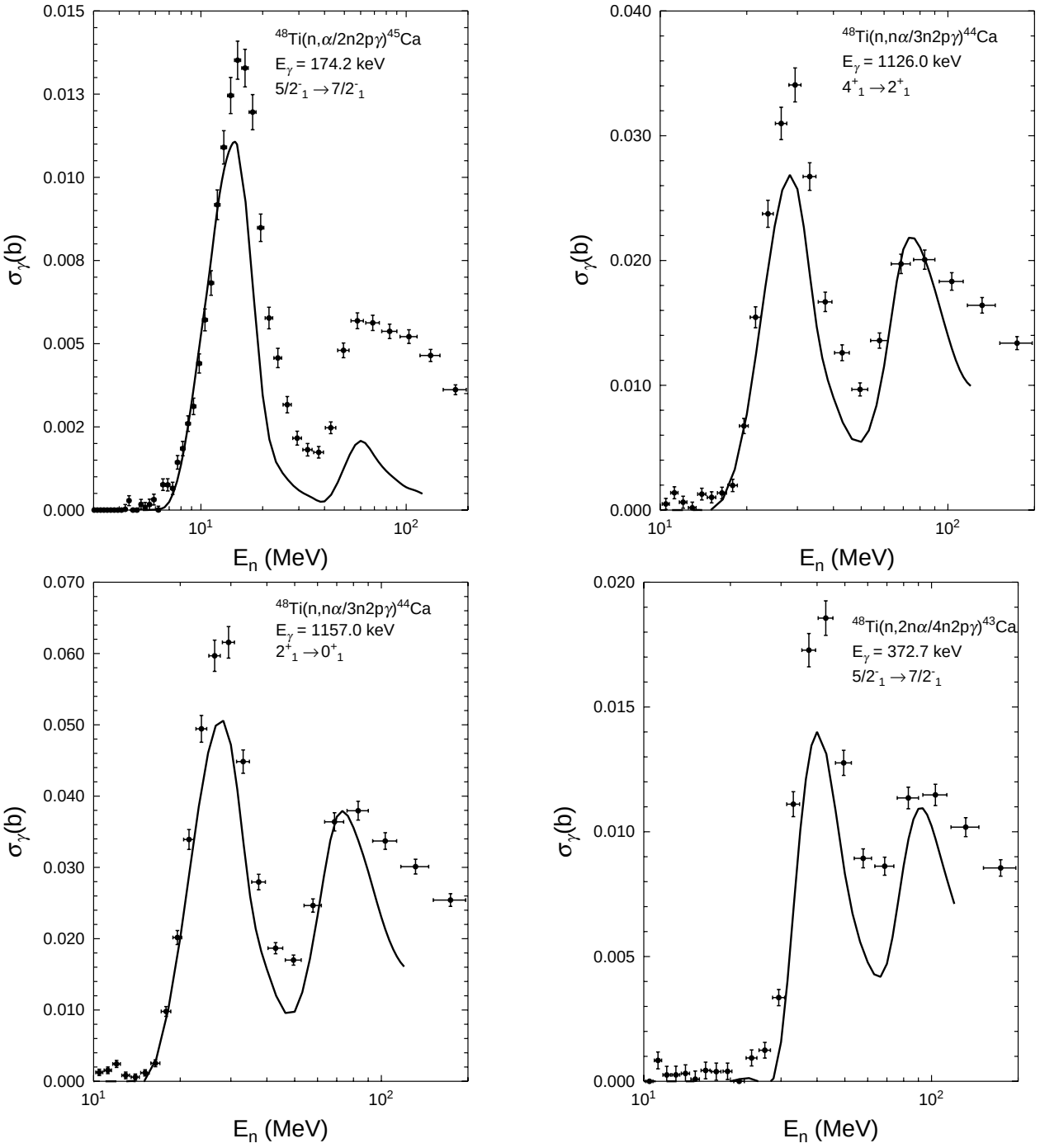
^{48}Ti(n,α/2n2pγ)^{45}Ca
E$_\gamma$ = 174.2 keV
5/2$^-_1$ → 7/2$^-_1$
^{48}Ti(n,nα/3n2pγ)^{44}Ca
E$_\gamma$ = 1126.0 keV
4$^+_1$ → 2$^+_1$
^{48}Ti(n,nα/3n2pγ)^{44}Ca
E$_\gamma$ = 1157.0 keV
2$^+_1$ → 0$^+_1$
^{48}Ti(n,2nα/4n2pγ)^{43}Ca
E$_\gamma$ = 372.7 keV
5/2$^-_1$ → 7/2$^-_1$
σ$_\gamma$(b)
E$_n$ (MeV)

FIG. 9: